Structural comparison of two strains of foot-and-mouth disease virus subtype O_1 and a laboratory antigenic variant, G67

Susan Lea[1,2], Robin Abu-Ghazaleh[3], Wendy Blakemore[3], Stephen Curry[3†], Elizabeth Fry[1], Terry Jackson[3], Andrew King[2], Derek Logan[1‡], John Newman[3] and David Stuart[1,2*]

[1]Laboratory of Molecular Biophysics, Rex Richards Building, South Parks Road, Oxford OX1 3QU, UK, [2]Oxford Centre for Molecular Sciences, New Chemistry Laboratory, Oxford OX1 3QT, UK and [3]BBSRC Institute for Animal Health, Pirbright Laboratory, Ash Road, Pirbright, Woking GU24 0NF, UK

Background: Foot-and-mouth disease viruses (FMDVs) are members of the picornavirus family and cause an economically important disease of cloven-hoofed animals. To understand the structural basis of antigenic variation in FMDV, we have determined the structures of two viruses closely related to strain O_1BFS whose structure is known.
Results: The two new structures are, like O_1BFS, both serotype O viruses. The first, O_1 Kaüfbeuren (O_1K), is a field isolate dating from an outbreak of FMD in Europe in the 1960s. The second, called G67, is a quadruple mutant of O_1K, generated in the laboratory, that bears point mutations conferring resistance to neutralization by monoclonal antibodies, specific for each of the four major antigenic sites defined previously. The availability of the three related virus structures permits a detailed analysis of the way amino acid substitutions influence antigenicity. Structural changes are seen to be limited, in general, to the substituted side chain. For example, the GH loop of VP1, a highly antigenic and mobile protuberance which becomes ordered only under reducing conditions, was essentially indistinguishable in the three viruses despite the accumulation of up to four changes within its 15-residue sequence. At one of the other antigenic sites, however, changes between the two field strains did perturb both side-chain and main-chain structures in the vicinity.
Conclusions: The conservation of conformation of the GH loop of VP1 adds to the evidence implicating an integrin as the cellular receptor for FMDV, since this loop contains a conserved RGD (Arg-Gly-Asp) sequence structurally similar to the same tripeptide in some other integrin-binding proteins. Structural changes required for the virus to escape neutralization by monoclonal antibodies are generally small. The more extensive type of structural change exhibited by the field isolates probably reflects differing selective pressures operating *in vivo* and *in vitro*.

Structure 15 June 1995, **3**:571–580
Key words: antigenicity, evolutionary strategies, foot-and-mouth disease virus, picornavirus structure

Introduction

Foot-and-mouth disease viruses (FMDVs) constitute the aphthovirus genus of the Picornaviridae and cause an economically important disease of cloven-hoofed animals, especially cattle. The viruses are extremely infectious and replicate rapidly so that the main immune defence against infection is humoral, requiring high levels of circulating neutralizing antibodies. Control of the disease has been achieved in most of Europe by systematic slaughter of infected or potentially infected animals and/or vaccination. Despite extensive vaccination programmes the virus remains enzootic in many parts of the world. Practical difficulties in the preparation and storage of the killed-virus vaccine hamper such vaccination programmes, which are further complicated by the remarkable antigenic diversity of the virus, presumably a response to the pressure from the host's immune system. Isolates of FMDV have been grouped into seven serotypes, O, A, C, Asia, SAT-1, SAT-2 and SAT-3. Immunization of an animal with a virus from one of these serotypes provides no protection against infection with a virus of another serotype. Serotypes can be further divided into subtypes (more than 65 [1]) and strains by examination of the patterns of reactivity with individual monoclonal antibodies (MAbs).

As a picornavirus, FMDV is a non-enveloped, icosahedral virus of ~300 Å diameter and the protein capsid encloses a single-stranded RNA genome. The structures of several picornaviruses have been determined [2–7] revealing a highly conserved architecture. The capsid is composed of 60 copies of each of four viral proteins, VP1–VP4. Proteins VP1, VP2 and VP3 each consist of an eight-stranded β-barrel with a jelly-roll topology [8]. VP4 is less structurally conserved, and is entirely internal. The proteins are arranged on a T=1 icosahedral lattice. The surface of the virus consists largely of the loops joining the strands of the jelly rolls.

*Corresponding author. Present addresses: †Department of Biological Chemistry, Harvard Medical School, 240 Longwood Avenue, Boston MA 02115, USA and ‡Laboratory of Molecular Biology, Arrhenius Labs F3, Stockholm University, S-106 91 Stockholm, Sweden.

© Current Biology Ltd ISSN 0969-2126

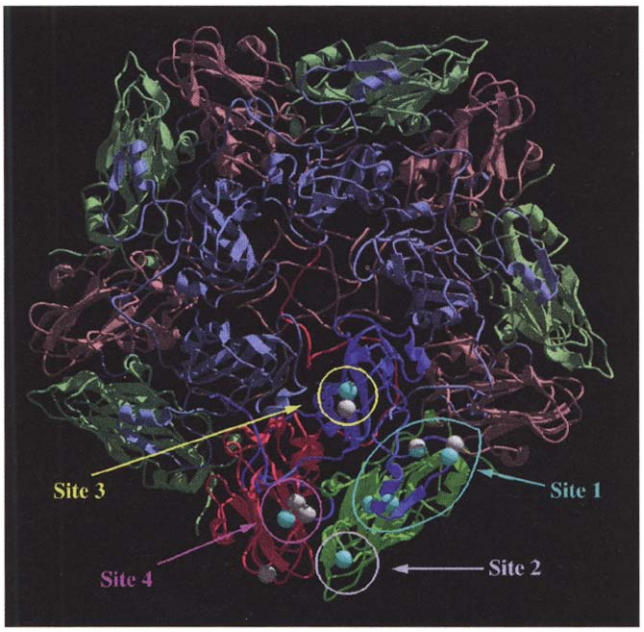

Fig. 1. A ribbon diagram showing the structure of a pentamer of FMDV type O_1K. The biological protomer is shown with standard colouring for the proteins (VP1, blue; VP2, green; VP3, red). The rest of the pentamer is shown in paler shades of these colours. The positions where the O_1 viruses discussed in this paper differ in amino acid sequence are shown as solid spheres on the protomer. The white spheres show where O_1K and O_1BFS differ and the cyan spheres where G67 differs from O_1K. Also indicated are the approximate locations of the four antigenic sites defined for type O FMDVs. Figure drawn using a modified version of MOLSCRIPT [43] (R Esnouf, unpublished) and rendered using RASTER3D [44].

Generation of MAb escape mutants (i.e. using selection with MAbs to induce mutations that confer resistance to, or 'escape' neutralization by that MAb) is the major method used to study antigenic variation of viruses *in vitro*. Many mutants have been produced and sequenced for FMDV [9–13] and other picornaviruses (e.g. human rhinovirus [14,15] and poliovirus [16,17]). These studies generally find that one, or only a very few, mutations are required to escape a single MAb, and that mutations induced by different antibodies may be grouped into antigenic 'sites'. Four such sites have been defined for type O_1 FMDVs (Fig. 1). Mutations induced by one MAb give protection against some of the other MAbs directed at the same site and no protection against MAbs directed at other sites.

Structural studies have shown that the surface area buried in the interface between an antigen and a binding antibody is approximately 700–800 $Å^2$ on each protein [18]. This is a large area of contact involving many amino acids. However, the interaction of any particular antibody is very specific, a single mutation often being sufficient to abolish binding [10,19]. Detailed analysis of a type C FMDV [20] suggested that strong structural constraints might 'filter out' many mutations which would disrupt the three-dimensional structure of the capsid. To investigate this further we have solved the structures of two type O_1 FMDVs, very closely related to the 1968 British Field Strain, O_1BFS, whose structure is known [5]. The first is a representative of the much-studied O_1 Kaüfbeuren (O_1K) strain. O_1K and O_1BFS were both circulating in Europe during the mid to late 1960s although they are South American in origin. Structural differences between these two viruses might be expected, therefore, to represent differences that have arisen 'in the field'. The selective pressure at work in the field, where viruses are neutralized by a complex polyclonal antibody response is different to that imposed *in vitro* by MAbs, which have higher affinity and greater specificity [21]. Thus, we would like to address the question, is the model for antigenic variation derived from isolating MAb escape mutants appropriate to the situation in the field? However, in this we face a significant difficulty: in practice the precise history of RNA viruses is complicated by the often uncertain 'passage histories' (the sequence of hosts in which the virus has replicated since isolation from the field) of the present-day viruses. It is therefore impossible to be certain that a particular difference seen between O_1BFS and O_1K represents the effects of field-imposed pressures rather than subsequent mutations. However, these two strains are considered to be relatively 'close to field' for laboratory strains and are clearly very closely related. The sequences of the two viruses differ by only five or six amino acids [10] in the four capsid proteins (Fig. 1).

We have also studied a laboratory-derived MAb quadruple escape mutant, designated G67. This virus was produced by sequential exposure of O_1K to MAbs directed at the four antigenic sites defined in type O_1 FMDVs [10,13,22], and sequencing shows it to contain escape mutations in each of these regions (Fig. 1). Despite these mutations, G67 is still recognized as a subtype O_1 virus by polyclonal sera (as are O_1K and O_1BFS).

In our original type O_1BFS FMDV structure [5] the major antigenic site, site 1, corresponding to the GH loop of VP1 (residues 134–158) and dubbed the 'FMDV loop', was disordered. This was especially disappointing as this loop also contains a conserved RGD (Arg-Gly-Asp) tripeptide implicated in receptor binding [23–25]. We have since shown that a procedure involving reduction of a disulphide bond between residue 134 of VP1 (at the start of the GH loop) and residue 130 of VP2 allows the loop to settle into an ordered conformation on the virion surface lying over VP2 [26]. In addition, this causes some rearrangement of the VP2 EF loop (residues 130–132) and the refolding of the VP3 GH loop (residues 172–180) away from the surface of VP2. The conformation observed for the GH loop and, in particular, the RGD tripeptide lends further support to the proposal that this region of the structure is directly involved in interacting with an integrin receptor [26]. Structures of O_1K and G67 have been determined in both native and dithiothreitol (DTT)-soaked forms to enable comparisons of the conformation(s) adopted by the VP1 GH loop to be made with that seen for O_1BFS [5,26]. It

Table 1. Sequence differences between FMDV strains O_1BFS and O_1K and between O_1K and G67.

Residue	O_1BFS	O_1K	H_2O accessibility in O_1BFS		Residue	O_1K	G67	H_2O accessibility in O_1BFS	
			Å^2	%*				Å^2	%*
VP1					**VP1**†				
56	Val	Ile	1	0	43	Thr	Lys	117	78
133	Glu	Gly	49	27	138	Arg	Lys	192	76
137	Ser	Asn	77	62	148	Leu	Arg	45	25
					150	Val	Ala	30	19
VP2					**VP2**				
		NONE			72	Ser	Asn	92	77
VP3					**VP3**				
56	Arg	His	33	13	58	Glu	Val	170	91
60	Gly	Asp	14	16					
68	Thr	Met	90	60					

*Percentage H_2O accessibility of residue X in O_1BFS is calculated as: (accessibility in O_1BFS)/(accessibility in G-X-G extended tripeptide)×100. †An additional difference is observed between O_1K and G67 at residue 133 of VP1 Gly (O_1K)→Gln (G67). Either G67 has reverted to glutamine (as in O_1BFS) or the O_1K virus used to produce the reduced O_1K crystals was not the parent of G67. The latter seems the more likely explanation as the parental O_1K population was found to be mixed with respect to this residue.

should be noted that although the VP1–VP2 disulphide is only present in type O_1 FMDVs a similar disorder of the FMDV loop has been observed in the three-dimensional structure of a type C virus [20].

Results

Structure of O_1K

The sequence of O_1K, as reported by Kitson *et al.* [10], differs from that of O_1BFS by five or six amino acid changes (Fig. 1). The uncertainty about the number of differences arises because the parental O_1K population was found to be mixed, some clones having glutamine at position 133 of VP1 (as in O_1BFS) and some having a glycine at this position. Difference maps calculated between O_1K and O_1BFS (non-reduced) show clear areas of difference density corresponding to the four sequence changes outside the disordered FMDV loop region (Table 1, Fig. 2). The Val→Ile change at residue 56 of VP1 is marked by a small peak of positive density associated with the increase in side-chain length (Fig. 2a). This change is unlikely to be important in determining antigenic differences between O_1K and O_1BFS as the residue is buried in a hydrophobic pocket (the Cδ1 atom occupies a volume of 24 Å^3 which was previously unoccupied) within the capsid and is therefore inaccessible to antibody attack (water accessibilities [27] for all the altered amino acid positions are given in Table 1). A similar positive peak marks the change from threonine to methionine at residue 68 of VP3 (Fig. 2b) although this

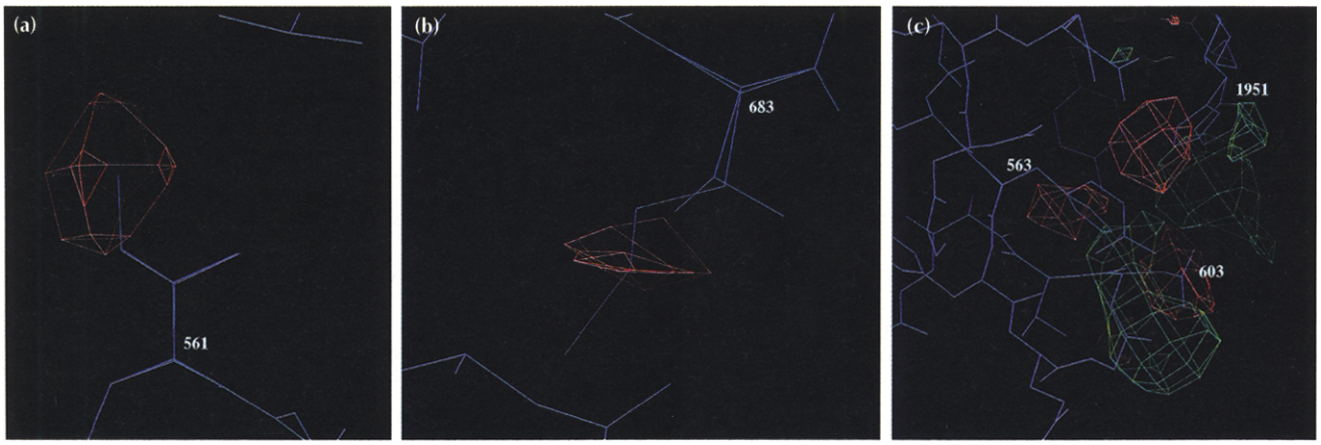

Fig. 2. Portions of the difference map calculated using amplitudes $|F_{O_1BFS}|-|F_{O_1K}|$ and phases (α_{O_1BFS}). Positive contours are shown in green and negative contours in red. All atom traces are shown for O_1BFS (dark blue) and O_1K (light blue). The residues are numbered, in this and subsequent figures, with the least significant digit denoting the protein to which the residue belongs (e.g. 561 is residue 56 of protein VP1). **(a)** Difference map contoured at ±3σ clearly showing the density associated with the change at position 56 of VP1 from threonine in O_1BFS to isoleucine in O_1K. **(b)** Difference map contoured at ±1.5σ showing the density associated with the change from threonine to methionine at position 68 of VP3. **(c)** Difference map contoured at ±3σ, showing the density associated with the two changes at positions 56 (Arg→His) and 60 (Gly→Asp) of VP3. The density associated with the movement of His195 of VP1 can also be seen. (Figure produced using program FRODO [40].)

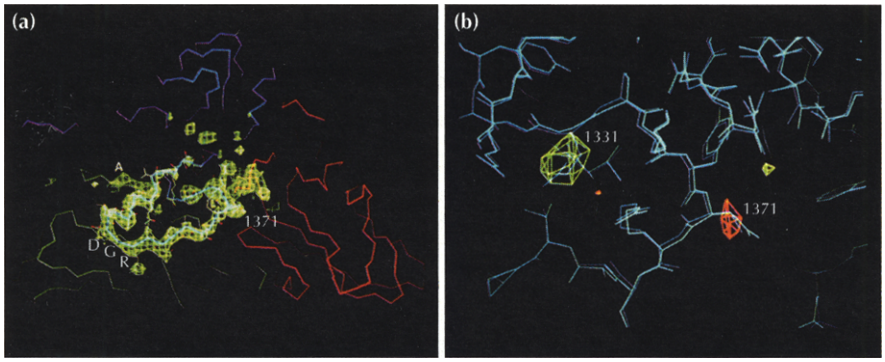

Fig. 3. The conformation of the FMDV loop in reduced O_1K. **(a)** Portion of the difference map calculated with amplitudes $|F_{O_1K(DTTsoaked)}| - |F_{O_1BFS(native)}|$ and phases (α_{O_1BFS}) contoured at $+2\sigma$. A Cα trace of a single protomer of O_1BFS is shown using the standard colour coding: VP1, blue; VP2, green and VP3, red. The largest feature is the density produced by the ordering of the GH loop of VP1 on reduction of the VP1–VP2 disulphide. The location of the RGD tripeptide implicated in receptor binding is indicated. **(b)** Portion of the difference map calculated with amplitudes $|F_{O_1BFS(DTTsoaked)}| - |F_{O_1K(DTTsoaked)}|$ and phases (α_{O_1BFS}) contoured at $\pm 2\sigma$. Positive contours are shown in green and negative contours are shown in red. All atom traces are shown for O_1BFS (dark blue) and O_1K (light blue). The density associated with the changes from Glu→Gly (133 of VP1) and Ser→Asn (137 of VP1) can be clearly seen. (Figure produced using FRODO [40].)

peak is perhaps smaller — it is only seen at the lower contour level of $+1.5\sigma$ — than might be expected for the gain of a sulphur atom. This is probably explained by the mobility of this residue (the crystallographic B-factors for all side-chain atoms of the threonine residue in O_1BFS exceed 50 Å^2). These are relatively small features in the difference maps. The major feature is an extended area of difference density around the mutations at residues 56 and 60 of VP3 (Fig. 2c), which lie close together on the viral surface. The substitution of a histidine for an arginine at residue 56 is associated with an area of negative density (shortening of the chain) and an area of positive density (accommodating the ring). The substitution at residue 60 of an aspartate for a glycine is clearly marked with a large area of positive density associated with the increase in side-chain length. The additional negative density observed in this region implies loss of the sulphate ion bound to Arg56 in O_1BFS [28] and loss of two water molecules from the area. The side chain of His195 near the C terminus of VP1 (which lies close to this region in the direction of the local fivefold axis of the icosahedron) also moves in response to the mutations in VP3. In addition to this connected series of side-chain and solvent movements, some slight, but significant, rearrangements of the polypeptide backbone also occur. These seem to be explained by a slight 'packing down' of these surface residues in O_1K relative to O_1BFS. Thus, residues 195 and 196 of VP1 are slightly more ordered as is Asp60 of VP3 (in spite of the lack of clear electron density for much of the side chain of this residue in $2F_o-F_c$ maps).

The difference map calculated between reduced O_1K and reduced O_1BFS confirms the changes in regions outside the GH loop of VP1 as well as showing that the FMDV loop adopts the same conformation in O_1K as in O_1BFS on reduction of the disulphide bond linking residue 130 of VP1 and residue 134 of VP2 (Fig. 3a). The two areas of difference density associated with the loop residues show that the virus from which the crystals have been grown contains the Glu→Gly mutation at position 133 of VP1 in addition to the Ser→Asn mutation at residue 137 (Fig. 3b). The difference density for both these changes shows that the differences are limited to alterations in the side chain, with no detectable movements of main-chain atoms. The order and degree of occupation of the FMDV loop in the reduced conformation have been investigated (see the Materials and methods section). The results indicate that, under reducing conditions, this ordered conformation is essentially fully occupied (occupancy no lower than 0.85).

Structure of G67

G67 differs from the parental O_1K by a further six mutations (Table 1). Three of the differences occur in the loop region (between residues 134 and 158) and are therefore only seen in maps calculated using data collected from the crystals treated with the reducing solution. The mutations can all be clearly seen (Fig. 4), marked by appropriate difference density associated with the side chains of the mutated residues. There is no evidence for any movement of main-chain atoms. Replacement of the threonine residue at position 43 of VP1 with a lysine is marked by density associated with the increase in length of this surface-exposed side chain (Fig. 4a) as is the change from serine to asparagine at residue 72 of VP2 (Fig. 4b). Conversely, the density associated with residue 58 of VP3 indicates a shortening of the side chain as would be expected for a change from glutamine to valine (Fig. 4c). Despite the location of residue 58 of VP3 between the two changes (at positions 56 and 60) seen to provoke large structural changes between O_1K and O_1BFS, the structural effects of this mutation appear to be limited to alteration of the side chain of residue 58. The GH loop of VP1 once more adopts the same main-chain conformation in the reduced structure, despite radical substitutions at three positions in the loop (Fig. 4d). This is somewhat unexpected as the Leu148→Arg mutation in VP1 involves a residue directed inwards into a hydrophobic pocket in the surface of VP2 in the reduced O_1BFS structure. The change from a leucine to a polar arginine might therefore be expected to alter the way in which the loop packs against the surface of VP2 in the reduced O_1BFS structure. The difference density (Fig. 4e), shows that this is clearly not the case, the structural changes being restricted to the side chain. The arginine side chain is easily accommodated

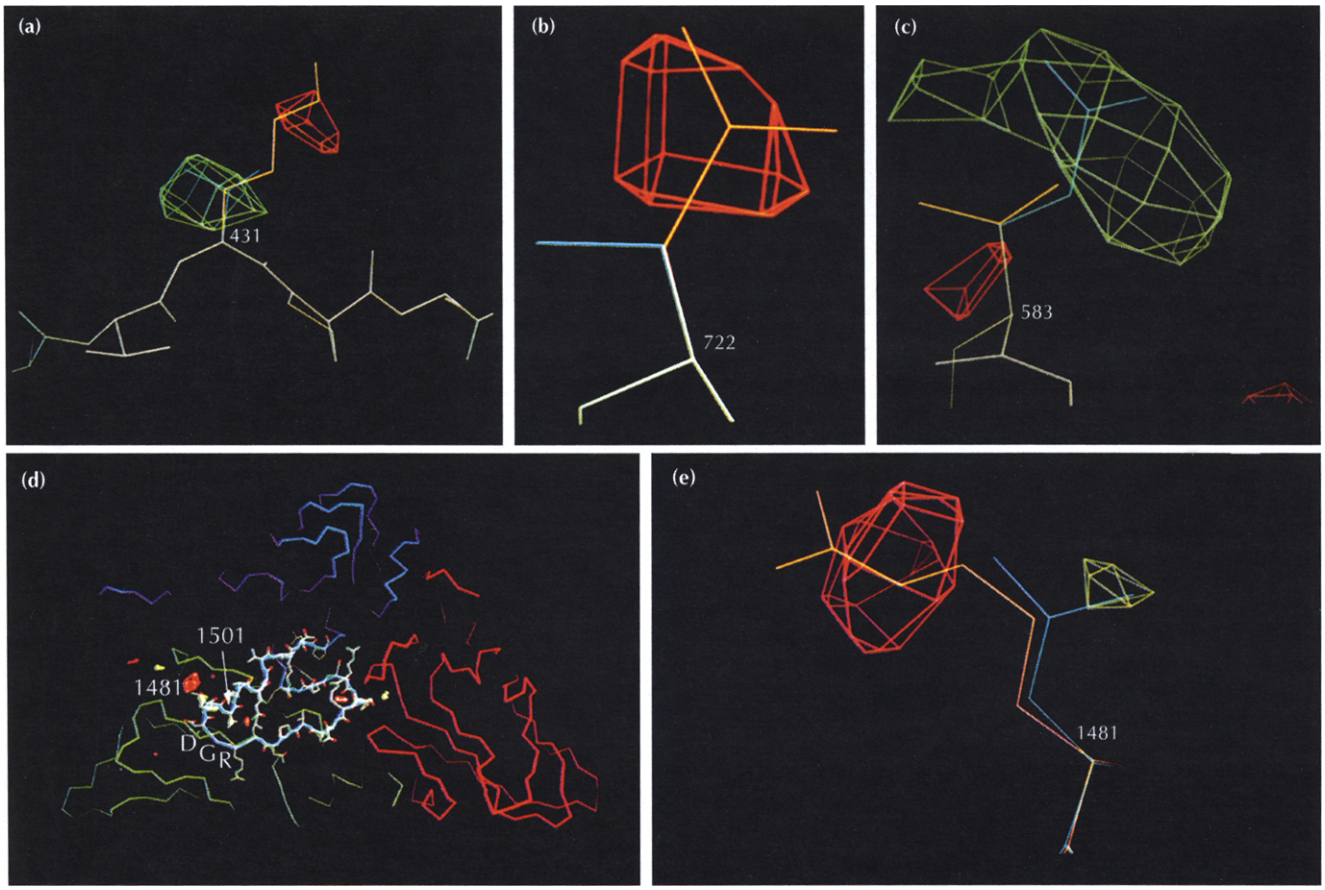

Fig. 4. Portions of the difference map calculated with amplitudes $|F_{O_1K(DTTsoaked)}| - |F_{G67(DTTsoaked)}|$ and phases (α_{O_1BFS}). Positive contours are shown in green and negative contours in red. All atom traces are shown for O_1K (light blue) and G67 (yellow). **(a)** Thr→Lys at position 43 of VP1, contoured at ±1.5σ. **(b)** Ser→Asn at position 72 of VP2, contoured at ±1.5σ. **(c)** Glu→Val at position 58 of VP3, contoured at ±1.5σ. **(d)** The density associated with the entire GH loop of VP1. The location of the RGD tripeptide implicated in receptor binding is highlighted by the one-letter code of the tripeptide residues. Map contoured at ±2σ. **(e)** Close-up view of the Leu148→Arg change within the GH loop of VP1, contoured at ±2σ. (Figure produced using FRODO [40].)

as the atoms beyond Cδ are directed away from the hydrophobic pocket, back up towards the capsid surface, lying over VP2 (Fig. 5).

Discussion

Receptor binding

The GH loop of VP1 is not only the major antigenic site but also contains the main receptor-binding determinant — an RGD tripeptide at the tip of the loop [23–25]. RGD is a recognition signal commonly used by adhesion molecules of the integrin family, and the almost perfect conservation of this RGD in FMDVs, especially given the great sequence variability elsewhere in this loop, gave the first clue that the cellular receptor for FMDV might be an integrin. This was supported by the ability of RGD-containing peptides to inhibit virus attachment to cells [23,24] and by the recent observation that an antibody directed against the human integrin, vitronectin, can also inhibit cell attachment [25]. We have shown previously [26] that the RGD tripeptide at the tip of the loop, in its ordered (reduced) form, adopts an extended conformation resembling the same motif in some other proteins that bind integrins in an RGD-dependent manner. This conformation of the RGD tripeptide, however, differs from those seen in non-integrin-binding proteins. It is thus striking, in the present studies, that the detailed structure of the loop is so highly conserved among the three viruses, especially in the conformation and orientation of its RGD tripeptide, despite the mobility of the loop and the accumulation within it of up to four mutations. Integrin specificity has been linked to the precise conformation of the main-chain and side-chain atoms of the RGD tripeptide [29]. The conservation of the way in which this short sequence is presented amongst these three O_1 viruses, despite changes within the sequence of the presenting loop (which might naively have been expected to alter the conformation) reinforces our view that integrin–ligand interactions may require specific, conserved, structural features.

Although the FMDV loop was similarly disordered in the structure of a type C FMDV [20], lacking the VP1–VP2 disulphide that destabilizes the loop conformation in the O_1 FMDVs, the recent determination of the structure of a peptide from the FMDV loop of a serotype C virus (which differs in 80% of its amino acids and contains four

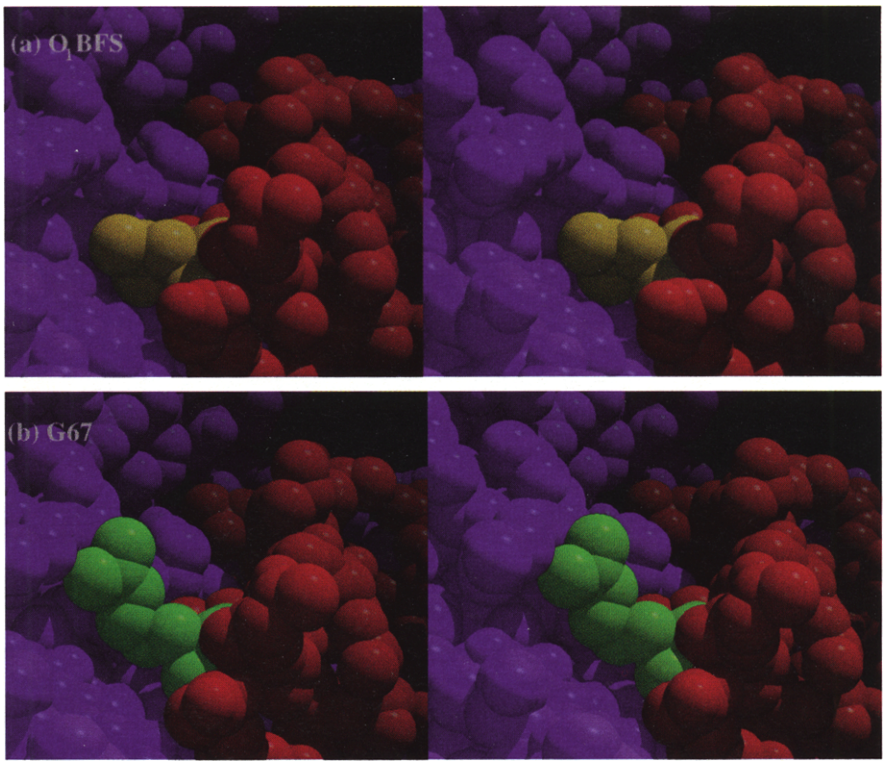

Fig. 5. Stereo space-filling representations of the capsid surface around residue 148 of VP1 to show the way in which this residue packs against the surface. Atoms of the GH loop of VP1 are coloured red with other atoms shown in purple. The view is approximately parallel to the surface of the virion. **(a)** The structure as observed in O_1BFS and O_1K where there is a leucine (yellow) at position 148. **(b)** The structure as observed in G67 where residue 148 of VP1 is an arginine (green).

deletions with respect to the corresponding loop in O_1BFS) in complex with an Fab fragment [30] reveals that this chemically different loop adopts a structure very similar to that described for reduced O_1 viruses. Structural predictions based on the propensity of different amino acids to form secondary-structural elements do not suggest that GH loops from different FMDVs should adopt either the particular structure revealed crystallographically [26,30] or even that they should adopt similar structures (data not shown). The conservation of overall structure in different environments and from different loops is therefore a little surprising and seems to imply that this long loop acts essentially as a separate domain hinged to the rest of the capsid at a point close to the disulphide bond in the 'oxidized' type O_1 virus and that it is disordered in other types of FMDVs by some less well understood mechanism. Such a role for the loop would explain the unusual results of Parry *et al.* [31] where, in contrast to our present observations, escape mutations appeared to act indirectly, subtly perturbing the balance of orientations of this loop with respect to the rest of the structure. Refinement of the loop structure in O_1K with the correct occupancy and a novel 'weighted' bulk solvent mask (see the Materials and methods section), shows that the RGD amino acids (residues 145–147) are the least mobile of the loop residues (Fig. 6) — despite their location at the tip of this very mobile loop — consistent with receptor specificity being linked to the conformation of this tripeptide.

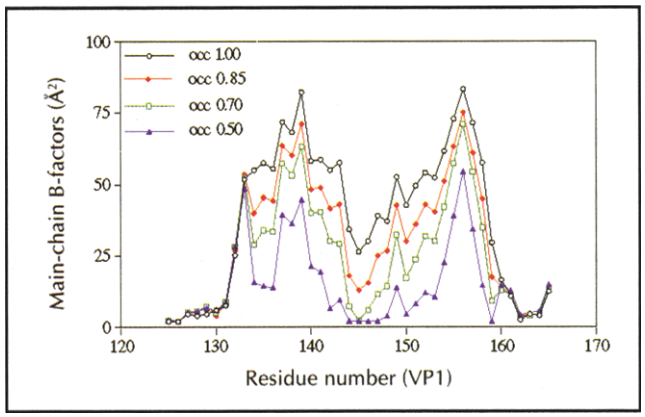

Fig. 6. Main-chain isotropic B-factors refined in X-PLOR [40] against all data in the range 20–3.3 Å for residues in the GH loop of VP1 after repeated refinements with different loop occupancies and application of the 'weighted' bulk solvent mask. The levels of occupancy are shown in different colours.

G67 crystal packing

The O_1K crystals belong to space group I23, and are essentially isomorphous with the O_1BFS crystals [5]. However, the G67 crystals are twinned such that the diffraction data possess the symmetry of space group I432. The increase in symmetry of the data collected from crystals of G67 can be understood in terms of an ambiguity arising in the way in which virions pack within the crystal lattice. For virions packing within space group I23 there are two possible ways in which the twofold axes of the virion can be aligned with the crystallographic twofold and threefold axes (Fig. 7). Within crystals of O_1K and O_1BFS, all the particles within a single crystal adopt the same orientation, whereas in our crystals of G67, 50% of the virions adopt one orientation and 50% the other. We have shown previously [32] that these crystals consist of a mosaic of blocks that contain similarly oriented virions, with the orientation differing

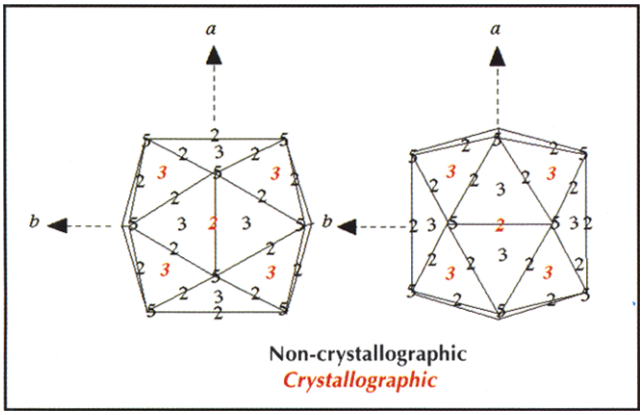

Fig. 7. Diagrammatic representation of the two orientations that can be adopted by an icosahedron on a point of 23 symmetry. Twofold and threefold crystallographic symmetry axes are indicated in red italicized text and two-, three- and fivefold NCS axes are in black.

between neighbouring blocks. When the orientations are averaged over the entire crystal volume, this distribution leads to additional (fourfold) symmetry within the data. The Ser72→Asn mutation in VP2 is the likely cause of the altered packing of the G67 crystals. The I23 packing interaction consists of stacking of the serine side chain over the side chains of Asp68 and Gln196 of VP2 from a symmetry-related virion. A fairly tight junction is formed with a pair of equivalent interactions making up the crystal contact. Modelling of the I23 and I432 packing interactions for G67 suggests that, rather than the interaction between the virion and the 90°-related virion becoming more favourable in the G67 crystals (there is no obvious hydrogen-bonding partner for an asparagine at position 72 of VP2), the I23 interaction becomes less favourable (the contact region becoming somewhat 'crowded' with the larger asparagine side chain). This suggests that the forces holding the G67 crystals together are weaker than those involved in the true I23 crystals — which is consistent with the requirement for higher salt concentrations to crystallize G67 (see the Materials and methods section and [33]).

Antigenic structure

The changes occurring in G67 (relative to O_1K) as a result of MAb escape-driven point mutations are very limited, having effect only by alterations in the nature of the side chain and not requiring movement of the main chain to produce antibody escape. The majority of the escape mutations involve surface-oriented side chains (Table 1) and all the mutations involve either substitution for a bulkier side chain or changes in the charge, or both. Thus, it is relatively simple to rationalize the mechanism of antibody escape in terms of either direct steric interference with binding of the antibody by the mutated side chain or the loss of stabilizing hydrogen bonding or ionic interactions. The GH loop of VP1 carried three substitutions in G67 although one of these, Leu148→Arg is sufficient by itself to account for MAb resistance [10]. The structural basis for this antigenic change appears difficult to explain because the side chain of this residue is directed inwards in O_1K and is not obviously exposed to antibody attack in the reduced structure. Predictions based on the reduced O_1K structure might have suggested that the effect of this mutation would be to alter the main-chain conformation of the GH loop. In fact this is not the mode of action. Instead, the larger arginine side chain is easily accommodated, not within the hydrophobic pocket but on the surface of VP2, directed towards the fivefold axis (Fig. 5). As the arginine side chain is more exposed than the leucine it may interfere with binding of a MAb directed at this region and capable of recognizing the loop in the reduced conformation. This is consistent with observations in other systems (e.g. in studies of neuraminidase escape mutants [34]) that relatively limited structural changes produce mutants capable of escape from MAbs. It must be remembered, however, that loop-directed MAbs may recognize the loop in some orientation other than that seen in the reduced virus and care should be taken in using the reduced virus structure to interpret escape from loop-binding MAbs.

The area of largest structural change between the two field-derived strains, O_1K and O_1BFS, is associated with the changes at residues 56 and 60 of VP3 (Fig. 2c). The Arg56→His mutation has important structural implications, the change in charge leading to loss of the bound sulphate ion and two water molecules from the region, and hence movement of His195 of VP1 which lies close by. A difference between the mutations at positions 56 and 60 of VP3 in O_1K and the MAb-driven G67 mutations is evident if the accessibility of the residue replaced is considered. The antigenically relevant G67 mutations (except at residue 148 of VP1 in the GH loop) all occur at very exposed residues having solvent accessibilities exceeding 75% of the maximum possible. By contrast, the O_1K mutations at 56 and 60 of VP3 occur at less exposed residues with accessibilities less than 20% of the maximum possible. By comparison with the MAb-induced mutations, which result only in alterations of side-chain structure, the mutations in O_1K affect less exposed residues and appear to cause a greater structural perturbation. Thus, the changes in side-chain structure are accompanied by some minor alterations in the structure of the polypeptide backbone in this region, leading to a slightly more rigid packing of the surface residues in O_1K. In addition to the change in charge caused by the mutation at residue 56, it seems plausible to suppose that the negative charge contributed by Asp60 in O_1K also contributes to increased packing rigidity, facilitating interactions between residues 195 of VP1 (histidine) and 56 of VP3 (histidine in O_1K and arginine in O_1BFS). Finally, it is interesting to note that residue 56 of VP3 is very variable amongst O_1 viruses, flipping between arginine and histidine both in the field and with passage *in vitro* (N Knowles, personal communication). As such a variable residue, it has often been thought of as structurally and antigenically unimportant; however, based on the

observed structural differences we predicted that MAbs directed at site 4 (see Fig. 1) would distinguish between O_1BFS and O_1K. This has been tested using MAb 14EH9 [10], which does indeed distinguish the two viruses, binding to O_1K but not to O_1BFS (J Crowther, personal communication), confirming that the structural alterations are antigenically significant. Maintaining variability at this position within the virus population in the field enhances the antigenic variation of the population, reducing the chance of a virus being cleared by an antibody directed at this site.

Biological implications

Foot-and-mouth disease is an extremely infectious and economically important disease of cloven-hoofed animals, which is caused by a small spherical RNA virus of the picornavirus family. As protective immunity is largely mediated by circulating antibody, the wide antigenic variation exhibited by these viruses — especially their noted propensity for undergoing sudden switches in antigenicity — complicates attempts to control the disease by vaccination.

The structures of the three related variants of the O serotype studied here (two field isolates and one derived by monoclonal antibody-driven mutation *in vitro*) reveal how individual amino acid substitutions are selected for their ability to confer resistance to neutralization by antibodies without compromising the structural or functional integrity of the virion. Thus, for each of the *in vitro*-derived mutations, the substitution of a single side chain by another of differing size or charge is sufficient to disrupt antibody recognition, without any consequential repacking of the surrounding protein. This rule applies even to the long hypervariable loop, the GH loop of viral protein 1 (VP1), that serves as the site of cell attachment. Recent evidence implicates one of the integrins, an important family of cell-adhesion molecules, as a receptor for the virus, binding being mediated by an essential RGD (Arg-Gly-Asp) tripeptide within the loop. Our comparative studies show that this loop can, despite its intrinsic mobility, tolerate numerous mutations that prevent binding of specific monoclonal antibodies while retaining an unaltered main-chain conformation, including the functionally active RGD at its tip. It may be significant that the one antigenic change that was accompanied by more extensive rearrangement, was one that was observed between the two field-isolated strains, and it remains possible therefore, that this structurally more disruptive mutation is more representative of the type of antigenic change elicited by the complex immune pressures operating *in vivo*.

Materials and methods

Virus growth and purification

Viruses were supplied by Dr G Belsham and grown on BHK-21 cell monolayers. Harvesting and purification followed our standard procedures [33,35].

Crystallization

Crystals of O_1K were grown by microdialysis against 11–12% saturated $(NH_4)_2SO_4$ as previously described [33]. Crystals of G67 required 21–23% saturated $(NH_4)_2SO_4$. Virus concentrations in the range 5–20 mg ml^{-1} were used in all cases. Crystals of both viruses grew as rhombic dodecahedra (as previously described for O_1BFS). However the crystals of G67 typically had dimensions of $0.4\times0.4\times0.2$ mm^3, approximately twice the size of the crystals of O_1K. Disulphides were reduced by soaking the crystals in 10 mM DTT, as described in [26].

Data collection

Data were collected at the SERC Synchrotron Radiation Source facility at Daresbury, UK. Experiments were performed at a constant temperature, usually 21°C, using stations 7.2, 9.5 and 9.6. Data collected on stations 7.2 and 9.6 were recorded photographically with an Arndt–Wonacott rotation camera using CEA X-ray film. These data were collected using the American method [36], as most crystals survived only one or two exposures in the beam. On station 9.5, data were collected on an 18cm diameter Mar Research Hendrix–Lentfer imaging plate device. The increased sensitivity of this device to λ=0.89 Å radiation permitted data collection from smaller crystals and permitted mulitple exposures from each crystal. Typically data were collected over a 0.5° oscillation at 1° intervals.

Data processing

Examination of the films/images appeared to indicate that both O_1K and G67 had crystallized isomorphously with O_1BFS in space group I23 with unit cell dimensions of a=b=c=345.0 Å, $\alpha=\beta=\gamma=90°$. Data processing followed our standard procedures [5,37]. A mis-packing of the G67 crystals [32] resulted in the data possessing higher symmetry than is physically possible for virions packed in a unit cell of these dimensions. Thus, processing the data as space group I432 gave R_{merge} values equivalent to those seen for processing the O_1K data as space group I23 (Table 2), although this mis-packing results in a twofold loss of information.

Table 2. Data processing statistics.

Data set	Native O_1K	Reduced O_1K*	Native G67	Reduced G67
Space group	I23	I23	I432†	I432†
No. of crystals exposed	27	2	19	23
No. of useful film packs/images	27	14	18	23
Minimum Bragg spacing collected (Å)	2.6	3.3	3.0	3.0
No. of reflections collected	237674	82112	101615	165285
No. of unique reflections	138727	58738	52219	64004
R_{merge}% (all data)‡	11.3	21	19	11.3
Completeness (%)	67	58	76§	92§

*Data collected using a Mar Research imaging plate, all other data collected on film. †N.B. due to crystal twinning. ‡$R_{merge}=[\Sigma_h\Sigma_i|(I_h-I_{hi})|/\Sigma_h\Sigma_i I_{hi}]\times100$. §Crystal twinning (see section 'G67 packing') results in a twofold loss of information.

Calculation of difference maps

As O_1K crystallized isomorphously with O_1BFS we felt the easiest way to visualize the differences between the two viruses would be by the calculation of difference maps (which are extremely sensitive to small shifts in atomic positions [38]). Reflections were matched and scaled, in resolution shells, to observed amplitudes for the other O_1 viruses (Table 3). These scaled reflections were then matched with the 'best' O_1BFS native phases — produced after 719 cycles of non-crystallographic symmetry (NCS) averaging [5,39]. Maps were calculated with coefficients: $|F_{virus1}|-|F_{virus2}|,\alpha_{O_1BFS}$ at 3.5 Å and 4.0 Å and then averaged over the five NCS-related icosahedral subunits within the crystallographic asymmetric unit. Calculation of difference maps using the G67 data was complicated by the mis-packing of the crystals. The data were processed in point group 432 and therefore could not be simply matched to the other O_1 data sets and the available phases. As previously described [32], pseudo-432 intensities calculated as the arithmetic mean of the I23 intensities for reflection pairs *h,k,l* and *k,h,l* provided an excellent model of the observed G67 data. Comparisons between the other O_1 viruses and G67 were therefore made by producing such pseudo-432 data sets for each virus which were scaled (as before with calculation of R_{match} and C_{match}; Table 3) to the G67 data. These scaled data were then 'unfolded' into I23 by duplication of reflection records and matched with the native O_1BFS phases to calculate difference maps (as for O_1K) in I23. After fivefold averaging, these maps were easily interpreted although somewhat noisier than the O_1K maps (reflected in the need to display lower contour levels to see the sequence changes, e.g. 1.5σ *versus* 3σ contours).

Table 3. Mean fractional isomorphous differences between X-ray data for the viruses studied.

	Native O_1K	Reduced O_1K	Native G67	Reduced G67
Native O_1BFS				
R_{match}*	13.9	19.7	15.0	13.5
C_{match}†	94.0	88.2	87.6	90.3
Reduced O_1BFS				
R_{match}*	17.2	17.8	15.8	10.9
C_{match}†	91.2	90.0	86.6	93.6

$$*R_{match}=\Sigma_h||F_{virus1}|_h-|F_{virus2}|_h|/\Sigma_h|F_{virus1}|_h$$

$$^{\dagger}C_{match}=\frac{\Sigma_h(\langle F_{virus1}\rangle-|F_{virus1}|_h)(\langle F_{virus2}\rangle-|F_{virus2}|_h)}{\sqrt{[\Sigma_h(\langle F_{virus1}\rangle-|F_{virus1}|_h)^2\cdot\Sigma_h(\langle F_{virus2}\rangle-|F_{virus2}|_h)^2]}}$$

Model building

Models have been built of both mutants (using FRODO [40]) by replacement of the mutated residue and movement of the side chain to satisfy the difference density and Fourier maps, as appropriate. Refinement of these structures was not performed as there was little significant movement of main-chain atoms.

Refinement of the occupancy of the GH loop of VP1 using a novel 'weighted' bulk solvent mask

Some refinement has been performed using the reduced O_1K data and model to further investigate the occupancy of the mobile GH loop of VP1. Estimation of the occupancy of mobile features can be complex [41]. However, we had previously investigated the occupancy of the GH loop of VP1 in the reduced O_1BFS virus by independent refinements with different loop occupancies which led us to estimate the occupancy at 80% [26]. To investigate this further, a model of reduced O_1K (based on the refined structure of reduced O_1BFS) was built in FRODO [40] and refined using version 3.1 of X-PLOR [42] with an occupancy-weighted bulk solvent mask. The bulk solvent correction in this version of X-PLOR sets all grid points in the fast-fourier transform calculation that are not specified as belonging to protein equal to a uniform electron density (in this case 1.0 e^- $Å^{-3}$) and stores the transform of this solvent mask in an array of partial structure factors, F_{part}. The corresponding F_{part} is vectorially added to each F_{PROT} (the calculated structure factor) before calculation of R-factors and so on:

$$F_{PROT}=F_{PROT}+K_pF_{part}e^{-B_p\sin^2\theta/\lambda^2}$$

The scale factor, K_p, and B-factor. B_p, may be chosen by a grid search. In this case values of K_p=0.32 and B_p=110 $Å^2$ were used. The presence, or absence, of a 24-residue loop will significantly alter the bulk solvent correction which will have a significant effect on the low-resolution data. As our data extend to a low-resolution cutoff of 20 Å we hoped to estimate accurately the occupancy of such features. To generate a 'weighted' bulk solvent mask two sets of F_{part} were generated, one appropriate to the native model (i.e. no ordered GH loop) and the other appropriate to the reduced model (i.e. with a model for residues 134–158 of VP1 and refolded loops in VP2 and VP3, see Introduction). These F_{part} values were then vectorially combined in such ratios as to enable correct refinement of structures with different loop occupancies. Fifty cycles of positional refinement and 30 cycles of individual, isotropic B-factor refinement were performed for four models with different loop occupancies, using the appropriate weighted bulk solvent mask. As expected, overall R-factors proved insensitive monitors (R_C=20% for all loop occupancies) in contrast to the experience of Grant *et al.* [41]. However, individual B-factors for the loop residues provided a sensitive test of the suitability of the chosen occupancy value. Refinements with loop occupancies of 0.5, 0.7, 0.85 and 1.0 gave markedly different B-factors for the residues within the mobile loops (Fig. 6). Occupancies lower than 0.85 led to B-factors for residues within the mobile loops refining to the minimum allowed value of 2.0 $Å^2$. As these loops would be expected to be relatively mobile, such low B-factors are indicative of an under-estimation of the occupancy. We therefore estimate the occupancy to be between 0.85 and 1.00. It is interesting to note that, when refined with these occupancy values, the amino acids of the RGD tripeptide, at the centre of the loop, have lower individual B-factors than any other loop residues (Fig. 6).

Coordinates have been deposited with the Brookhaven Protein Data Bank.

Acknowledgements: We thank the staff at DRAL for assistance during X-ray data collection; G Belsham for virus seed stocks; J Crowther for MAb anaylsis; N Knowles for useful discussions; R Bryan and R Esnouf for computing facilities and S Lee for help in preparation of the figures. EF and DL were supported by the Medical Research Council (MRC) and RA, SC and SL by the Biotechnology and Biological Sciences Research Council (BBSRC). The Oxford Centre for Molecular Sciences is supported by the BBSRC and the MRC. This work was, in part, supported by MAFF.

References

1. Pereira, H.G. (1977). In *Developments in Biological Standards* (Mackowiak, C. and Regamey, R.H., eds), vol. **35**, pp. 167–174, Karger, Basel.
2. Rossmann, M.G., *et al.*, & Vriend, G. (1985). Structure of a human common cold virus and functional relationship to other picornaviruses. *Nature* **317**, 145–153.
3. Hogle, J.M., Chow, M. & Filman, D.J. (1985). Three-dimensional structure of poliovirus at 2.9 Å resolution. *Science* **229**, 1358–1365.
4. Luo, M., *et al.*, & Palmenberg, A. (1987). The atomic structure of mengo virus at 3.0 Å resolution. *Science* **235**, 182–191.
5. Acharya, R., Fry, E., Stuart, D., Fox, G., Rowlands, D. & Brown, F. (1989). The three-dimensional structure of foot-and-mouth disease virus at 2.9 Å resolution. *Nature* **337**, 709–716.
6. Luo, M., He, C., Toth, K.S., Zhang, C.X. & Lipton, H. (1992). Three-dimensional structure of Theiler murine encephalomyelitis virus (BeAn strain). *Proc. Natl. Acad. Sci. USA* **89**, 2049–2413.
7. Grant, R.A., Filman, D.J., Fujinami, R.S., Icenogle, J.P. & Hogle, J.M. (1992). Three-dimensional structure of Theiler virus. *Proc. Natl. Acad. Sci. USA* **89**, 2061–2065.
8. Stuart, D.I. (1993). Viruses. *Curr. Opin. Struct. Biol.* **3**, 167–174.
9. Baxt, B., Vakharia, V., Moore, D.M., Franke, A.J. & Morgan, D.O. (1989). Analysis of neutralising antigenic sites on the surface of type A12 foot-and-mouth disease virus. *J. Virol.* **63**, 2143–2151.
10. Kitson, J.D.A., McCahon, D. & Belsham, G.J. (1990). Sequence analysis of monoclonal antibody resistant mutants of type O foot-and-mouth disease virus: evidence for involvement of the three surface exposed capsid proteins in four antigenic sites. *Virology* **179**, 26–34.
11. Pfaff, E., Muller, H., Haas, B. & Thiel, H.J. (1989). Molecular and immunological analysis of foot-and-mouth disease virus mutants. In Vaccines '89: Modern Approaches to New Vaccines Including Prevention of AIDS (Lerner, R.A., Ginsberg, H., Chanock, R. M. and Brown, F., eds), pp. 449–455, Cold Spring Harbour Laboratory, New York.
12. Thomas, A.A.M., Woortmeijer, R.J., Puijk, W. & Barteling, S.J. (1988). Antigenic sites on foot-and-mouth disease virus type A10. *J. Virol.* **62**, 2782–2789.
13. Xie, Q.-C., McCahon, D., Crowther, J.R., Belsham, G.J. & McCullough, K.C. (1987). Neutralisation of foot-and-mouth disease virus can be mediated through any of at least three separate antigenic sites. *J. Gen. Virol.* **68**, 1637–1647.
14. Sherry, B. & Rueckert, R.R. (1985). Evidence for at least two dominant neutralisation antigens on human rhinovirus 14. *J. Virol.* **53**, 137–143.
15. Sherry, B., Mosser, A.G., Colonno, R.J. & Rueckert, R.R. (1986). Use of monoclonal antibodies to identify four neutralisation epitopes on a common cold picornavirus, human rhinovirus 14. *J. Virol.* **57**, 246–257.
16. Page, G.S., Mosser, A.G., Hogle, J.M., Filman, D.J., Rueckert, R.R. & Chow, M. (1988). Three-dimensional structure of poliovirus serotype 1 neutralising determinants. *J. Virol.* **62**, 1781–1794.
17. Hogle, J.M. & Filman, D.J. (1989). The antigenic structure of poliovirus. *Philos. Trans. R. Soc. Lond. [Biol.]* **323**, 467–478.
18. Alzari, P.M., Lascombe, M. & Poljak, R.J. (1988). Three-dimensional structure of antibodies. *Annu. Rev. Immunol.* **6**, 555–580.
19. Tulip, W.R., Varghese, J.N., Webster, R.G., Laver, W.G. & Colman, P.M. (1992). Crystal structures of two mutant neuraminidase–antibody complexes with amino acid substitutions in the interface *J. Mol. Biol.* **227**, 149–159.
20. Lea, S., *et al.*, & Mateu, M.G. (1994). The structure and antigenicity of a type C foot-and-mouth disease virus. *Structure* **2**, 123–139.
21. Maddon, P.J., Littman, D.R., Godfrey, M., Maddon, D.E., Chess, L. & Axel, R. (1985). The isolation and nucleotide sequence of a cDNA encoding the T-cell surface protein T4: a new member of the immunoglobulin gene family. *Cell* **42**, 93–104.
22. McCahon, D., *et al.*, & De Simone, F. (1989). Evidence for at least four antigenic sites on type O foot-and-mouth disease virus involved in neutralisation; identification by single and multiple monoclonal antibody-resistant mutants. *J. Gen. Virol.* **70**, 639–645.
23. Surovoi, A.Y., Ivanov, V.T., Chepurkin, A.V., Ivanyuschenkov, V.N. & Dryagalin, N.N. (1988). Is the Arg-Gly-Asp sequence the site for foot-and-mouth disease virus binding with cell receptor? *Soviet J. Bioorg. Chem.* **14**, 965–968.
24. Fox, G., Parry, N.R., Barnett, P.V., McGinn, B., Rowlands, D.J. & Brown, F. (1989). Cell attachment site on foot-and-mouth disease virus includes the amino acid sequence RGD (arginine-glycine-aspartic acid). *J. Gen. Virol.* **70**, 625–637.
25. Berinstein, A., Roivainen, M., Hovi, T., Mason, P.W. & Baxt, B. (1995). Antibodies to the vitronectin receptor (integrin $\alpha_v\beta_3$) inhibit binding and infection of foot-and-mouth disease virus to cultured cells. *J. Virol.* **69**, 2664–2666.
26. Logan, D., *et al.*, & Stuart, D. (1993). Structure of a major immunogenic site on foot-and-mouth disease virus. *Nature* **362**, 566–568.
27. Lee, B.K. & Richards, F.M. (1971). The interpretation of protein structures: estimation of static accessibility. *J. Mol. Biol.* **55**, 379–400.
28. Fry, E., *et al.*, & Stuart, D. (1990). Architecture and topography of an aphthovirus. *Semin. Virol.* **1**, 439–451.
29. Pffaf, M., *et al.*, & Engel, J. (1994). Selective recognition of cyclic RGD peptides of NMR defined conformation by $\alpha_{IIb}\beta_3$, $\alpha_v\beta_3$, and $\alpha_5\beta_1$ integrins. *J. Biol. Chem.* **269**, 20233–20238.
30. Verdagauer, N., Mateu, M.G., Andreu, D., Giralt, E., Domingo, E. & Fita, I. (1995). Structure of the major antigenic loop of foot-and-mouth disease virus complexed with a neutralizing antibody: direct involvement of the Arg-Gly-Asp motif in the interaction. *EMBO J.* **14**, 1690–1696.
31. Parry, N., *et al.*, & Stuart, D. (1990). Structural and serological evidence for a novel mechanism of immune evasion in foot-and-mouth disease virus. *Nature* **347**, 569–572.
32. Lea, S. & Stuart, D. (1995). Deconvolution of fully overlapped reflections from crystals of foot-and-mouth disease virus O_1 G67. *Acta Crystallogr. D* **51**, 160–167.
33. Curry, S., *et al.*, & Stuart, D. (1992). Crystallisation and preliminary X-ray analysis of three serotypes of foot-and-mouth disease virus. *J. Mol. Biol.* **228**, 1263–1268.
34. Tulip, W., *et al.*, & Colman, P. (1991). Refined atomic structures of N9 subtype influenza virus neuraminidase and escape mutants. *J. Mol. Biol.* **221**, 487–497.
35. Fox, G., Stuart, D., Acharya, K.R., Fry, E., Rowlands, D.J. & Brown, F. (1987). Crystallisation and preliminary X-ray diffraction analysis of foot-and-mouth disease virus. *J. Mol. Biol.* **196**, 591–597.
36. Rossmann, M. & Erickson, J. (1983). Oscillation photography of radiation-sensitive crystals using a synchrotron source. *J. Appl. Crystallogr.* **16**, 629–636.
37. Collaborative Computational Project, Number 4 (1994). The CCP4 suite: programs for protein crystallography. *Acta Crystallogr. D* **50**, 760–763.
38. Blundell, T.L. & Johnson, L.N. (1976). *Protein Crystallography.* Academic Press, New York.
39. Fry, E., Acharya, R. & Stuart, D. (1993). Methods used in the structure determination of foot-and-mouth disease virus. *Acta Crystallogr. A* **49**, 45–55.
40. Jones, T.A. (1985). Interactive computer graphics: FRODO. *Methods Enzymol.* **115**, 157–171.
41. Grant, R.A., Hiremath, C.N., Filman, D.J., Syed, R., Andries, K. & Hogle, J.M. (1994). Structures of poliovirus complexes with anti-viral drugs: implications for viral stability and drug design *Curr. Biol.* **4**, 784–797.
42. Brünger, A.T. (1992). *X-PLOR Version 3.0.* Yale University, New Haven, CT.
43. Kraulis, P.J. (1991). MOLSCRIPT: a program to produce both detailed and schematic plots of protein structures *J. Appl. Crystallogr.* **24**, 946–950.
44. Merritt, E.A. & Murphy, M.E.P. (1994). Raster3D version 2.0. A program for photorealistic molecular graphics *Acta Crystallogr. D* **50**, 869–873.

Received: **28 Mar 1995**; revisions requested: **13 Apr 1995**; revisions received: **27 Apr 1995**. Accepted: **27 Apr 1995**.